JACS
JOURNAL OF THE AMERICAN CHEMICAL SOCIETY

ARTICLE

pubs.acs.org/JACS

Plasmon-Based Free-Radical Photopolymerization: Effect of Diffusion on Nanolithography Processes

Claire Deeb,[†] Carole Ecoffet,[‡] Renaud Bachelot,[†] Jérôme Plain,[†] Alexandre Bouhelier,[§] and Olivier Soppera*[,‡]

[†]Laboratoire de Nanotechnologie et d'Instrumentation Optique LNIO-ICD CNRS-UMR 6279, Université de Technologie de Troyes, Troyes, France

[‡]Institut de Science des Matériaux de Mulhouse (IS2M-CNRS LCR 7228), Université de Haute-Alsace, Mulhouse, France

[§]Laboratoire Interdisciplinaire Carnot de Bourgogne CNRS-UMR 5209, Université de Bourgogne, Dijon, France

ABSTRACT: This Article interrogates the mechanisms responsible for nanoscale photopolymerization induced by confined and enhanced electromagnetic fields. Surface plasmon dipolar resonance of individual Ag nanoparticles was used as an optical near-field source to locally trigger the reaction of a photopolymerizable formulation. Laser excitation of the nanoparticles embedded in the formulation reproducibly generates polymer features with typical dimensions ranging from 2 nm to a few tens of nanometer. We have determined the physicochemical parameters and mechanisms controlling the spatial extent of the photopolymerization process. We found that the diffusion of the dye is the main process limiting the polymerization reaction, as opposed to what is observed at the microscale with an equivalent chemical system. This approach demonstrates that plasmon-based polymerization can achieve true nanometer scale resolution and also provides a unique opportunity to investigate photochemistry at this length scale.

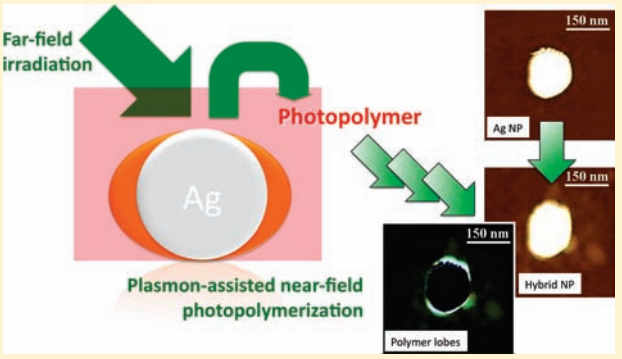

INTRODUCTION

Many efforts have been dedicated during past years to proposing innovative methods to push the limits and constraints of nanofabrication processes.[1] Among the large diversity of approaches, photolithography is still a method of interest; the recent improvement of far-field imaging beyond the diffraction limit[2−5] and smart control of local diffusion processes open the possibility to confine photochemical reactions at the nanoscale.[3] An alternative approach for controlling photolithography at these length scales consists of using plasmon resonances in metal nanostructures to confine and enhanced optical fields.[6] The plasmonic responses of metal nanoparticles are utilized in a large variety of applications including controlled excited-state dynamics,[7] plasmon lasing,[8] active optical antennas,[9] and biosensing.[10] Recently, plasmonic confinement and enhancement were also successfully used to induce a local photopolymerization reaction.[11−13] Photoinduced processes are of considerable interest for harnessing and controlling polymerization reactions at the nanoscale beyond chemical methods based on surface-confined living polymerization.[14] The approach can be effectively employed for designing hybrid nanostructures with polarization-dependent optical properties,[11] for quantitatively determining local electromagnetic field magnitude,[12] and for developing advanced subwavelength optical lithography techniques.

In this Article, we report on a parametric study of a photoinduced polymerization reaction confined at the nanoscale using a plasmonic nanosource and a free-radical photopolymerizable system. We demonstrate the possibility to create polymer structures down to 2 nm corresponding to a resolution of $\lambda/200$, well below the diffraction limit. Our results show that near-field photopolymerization can serve as a valuable analytical tool to understand the physicochemical parameters and mechanisms controlling the polymerization process. The method is based on analyzing the surface topology of the polymerized features under various conditions of irradiation and chemical compositions. In particular, we unambiguously emphasize the crucial role of dye diffusion at this length scale, as opposed to previous studies conducted at the micrometer level,[15,16] where its role was reasonably neglected. We clearly establish that, at this scale, the photopolymerization is not controlled by the local oxygen concentration that generally limits the polymerization process by inhibiting radicals. The local concentration of the dye involved in the radical creation is the limiting factor for the photopolymerization process.

Our work not only demonstrates that we can employ plasmonic responses to achieve nanometer-scale polymerized features, but also constitutes, from a more fundamental point of view, a unique opportunity to investigate photochemical reaction pathways at the nanometer scale.

EXPERIMENTAL METHODS

Ag Nanoparticles (Ag NPs) Deposition. Commercial colloidal silver (Ag) NPs, supplied by BBI with an average diameter of 60 nm and

Received: February 21, 2011
Published: May 27, 2011

 © 2011 American Chemical Society

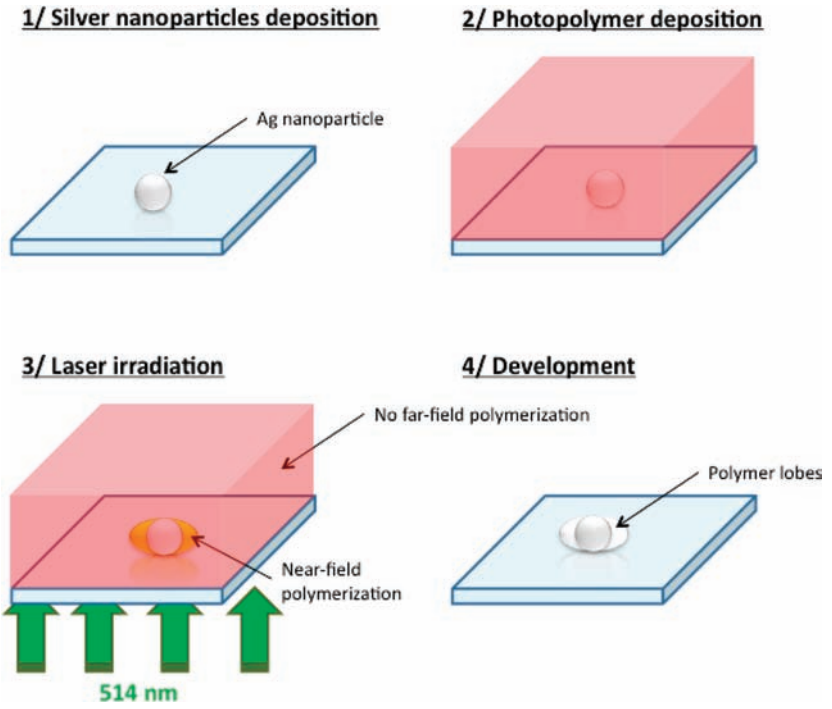

Figure 1. Schematic description of the procedure. Near-field photopolymerization is triggered by the plasmon response of the Ag nanoparticle. The hybrid metal/polymer particle is revealed after developing the formulation.

a surface plasmon resonance (SPR) at 460 nm in water were used here. A glass slide was immersed in a diluted Ag colloidal solution for 12 h to achieve a deposition of isolated nanoparticles (distance between two adjacent particles greater than 500 nm). The substrate was then rinsed with distilled water and dried with air.

To ensure an efficient anchoring of the nanoparticles on the glass slide, the substrate was previously functionalized to create an amine-terminated self-assembled monolayer on which silver nanoparticles, stabilized by citrate groups, were strongly bounded to the glass surface.

Photopolymerizable Formulation (PPF). The photopolymerizable formulation is composed of three components: a sensitizer dye (Eosin Y, 2′,4′,5′,7′-tetrabromofluorescein disodium salt, Aldrich), an amine (MDEA, methyldiethanolamine, Aldrich), and a multifunctional acrylate monomer, pentaerythritol triacrylate (PETIA, Sartomer). A 514 nm argon:krypton (Ar:Kr) laser wavelength was used in the experiments because it overlaps both the absorption spectrum of Eosin Y (EY) and the surface plasmon resonance of the Ag NP in the formulation. Upon irradiation with a wavelength lying in the EY absorption region, that is, 450−550 nm, the excited states of EY can react with MDEA to create free radicals.[17] PETIA was used as received from the supplier. The results reported here were obtained with mixtures containing 0.5% in weight of EY (which corresponds to 7×10^{-3} mol/L) and 4% in weight of MDEA (3×10^{-2} mol/L), unless mentioned differently.

Characterization of the PPF. The PPF was carefully characterized by spectroscopy and the threshold dose necessary to initiate the polymerization was systematically determined. Bleaching and polymerization kinetics were investigated by UV−visible spectroscopy and Fourier transformed infrared (FTIR) spectroscopy. Bleaching (%) and conversion ratio (%) correspond to the fraction of the dye (respectively monomer) that was consumed at a given irradiation time. These values were extracted, respectively, from the relative decrease of the EY absorbance in the UV−visible spectrum (evaluated at maximum absorption: 532 nm) and the C═C stretching band in the FTIR spectrum (1635 cm^{-1}).[16]

In parallel, a precise evaluation of the polymerization threshold was conducted. The threshold energy corresponds to the minimum energy necessary to observe polymer parts on the glass substrate. This parameter is of paramount importance to determine the energy necessary to trigger a near-field photopolymerization without significant chemical modifications induced by a far-field illumination.

Near-Field Photopolymerization. The procedure for near-field photopolymerization is depicted in Figure 1. The Ag NPs are deposited on the glass substrate. Intermittent-contact mode atomic force microscopy (AFM) is conducted to image the nanoparticles. By referring to landmarks placed on the sample surface, we have selected Ag NPs having reasonable in-plane symmetry (quasi-spherical) so that their diameters can be deduced from a height measurement. The particles are then covered with the photopolymerizable solution by simple drop casting. Illumination at 514 nm with a linearly polarized laser beam is performed under controlled power density and irradiation time. The irradiation dose is always chosen to be lower than the threshold energy (e.g., the dose needed to induce far-field polymerization). Under these conditions, no polymerization occurs in far-field, and only the optical field enhanced by the plasmon response of the Ag NP overcomes the threshold and initiates polymerization. The sample is then rinsed with ethanol and isopropanol to remove the unpolymerized monomer, thus revealing the hybrid nanoparticles. The selected Ag NPs are reimaged again to compare the particles before and after irradiation. By differentiating the images before and after the procedure, we can quantitatively characterize the extent of polymerization,[12] while circumventing the apparent increase of the nanoparticle width due to convolution with the AFM tip.

■ RESULTS AND DISCUSSION

The photoinitiating system composed of EY and the MDEA associated with an acrylate monomer was previously used in holography or laser direct writing self-guiding photopolymerization.[15−17] This system exhibits a suitable sensitivity at

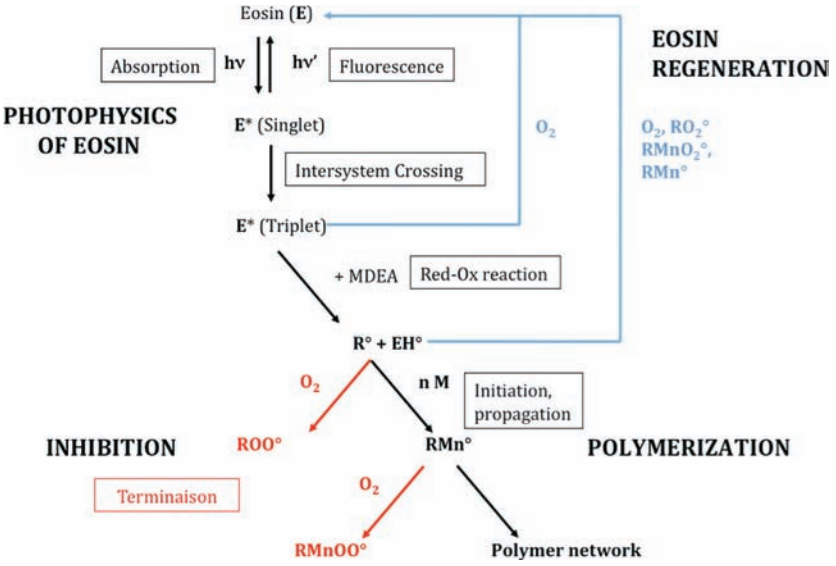

Figure 2. Scheme illustrating the photoinduced polymerization of the methacrylate monomer, the inhibition processes, and the eosin Y regeneration pathways.

514 and 532 nm. It is very flexible because the components can be modified independently to adjust the physical and the chemical properties of the formulation: viscosity, spectral sensitivity, and polymerization threshold.

A simplified scheme of the molecular pathway leading to photopolymerization is shown in Figure 2. The absorption of a photon leads to the excited singlet state of the EY, and then to the triplet state by intersystem crossing. From the triplet state, the dye can react with the amine to produce the first radical able to induce the free-radical polymerization of the methacrylate monomer. Because the monomer is trifunctional, a rapid cross-linking of the polymer network is usually observed.[18] The left part of the scheme describes all of the inhibition processes taking place. They are mainly due to the oxygen dissolved in the photopolymer. Oxygen can react with the triplet state of the dye, or with radicals, to create peroxide radicals that are not active for polymerization.[19] Usually, in free-radical polymerization, these later processes are considered to be detrimental. They decrease the efficiency of the global polymerization process by introducing an inhibition period and, in some cases, limit the final monomer conversion. However, in micro- and nanofabrication, such molecular phenomenon can be advantageously used to precisely control the polymerization volume. The consequence of the oxygen inhibition is the introduction of a threshold of polymerization that can be determined under precise conditions.[15]

Both pathways lead to the transformation of eosin to a protonated eosin radical. This radical is known to be ineffective for initiating polymerization. However, several reactions of this radical have to be considered:[20] first, it can react with another protonated eosin radical to regenerate an eosin molecule in the leuco form. The latter form is not absorbant at 532 nm, and the consequence of this reaction is the progressive bleaching of the eosin formulation. Second, the protonated eosin radical can undergo a disproportion reaction with other radicals (deprotonated amine radical, peroxide radicals, or free-radicals of the growing polymer chains). In this case, the eosin is regenerated to its fundamental state. Such process regenerates the eosin in an active state that can photosensitize again other MDEA reactions.

The precise AFM measurement of the lateral extension of the nanoparticles gives a quantitative measure of the spatial extension of the photopolymerization. Figure 3 shows a typical example demonstrating our ability to trigger a nanoscale photopolymerization. Figure 3a and b shows, respectively, the AFM images before and after the procedure. A spherical particle (circle) was selected for its apparent spherical shape before the procedure. Figure 3c and d represents, respectively, close-up images of the selected particle. The incident field polarization direction is represented by the white arrow shown in Figure 3b. The comparison between panels (a) and (b) demonstrates undoubtedly that the same particles can be observed before and after the polymerization process (including the development step), indicating a stable anchoring of the nanoparticles on the substrate surface. The change of particle morphology before and after polymerization is readily seen by comparing Figure 3c and d. The Ag NP exhibits an elongation in the direction of the incident field polarization resulting from polymerization of two lobes on either side of the particle. These lobes are revealed by the differential image presented in panel (e). The lateral distribution of the lobes is reminiscent of the intensity distribution of Ag NPs irradiated at its dipolar resonance with a linearly polarized light.[6,11]

Using the lateral extent of the lobes deduced from differential images, we investigated the role of irradiation dose on the polymerization. The data are plotted in Figure 4. The black curve was obtained by illuminating the nanoparticles at constant power ($1.4\ mW/cm^2$) . The irradiation time was varied between 0.1 and 0.9 s. This experiment gives a direct visualization of the growth kinetic of the polymer lobes. The dose is given in % of the threshold dose for polymerization. The dose was chosen lower than the threshold dose (100%) to ensure that no polymerization can occur due to the far-field irradiation. As expected, the polymer extension increases with irradiation time. Interestingly, the trend is almost linear. The width of the polymer lobes can be tuned between 3 and 18 nm, demonstrating the high control of the spatial extent of the polymerization reaction. It is remarkable to notice the unprecedented resolution ($\sim\lambda/200$) that is achievable with this plasmon-assisted photopolymerization process.

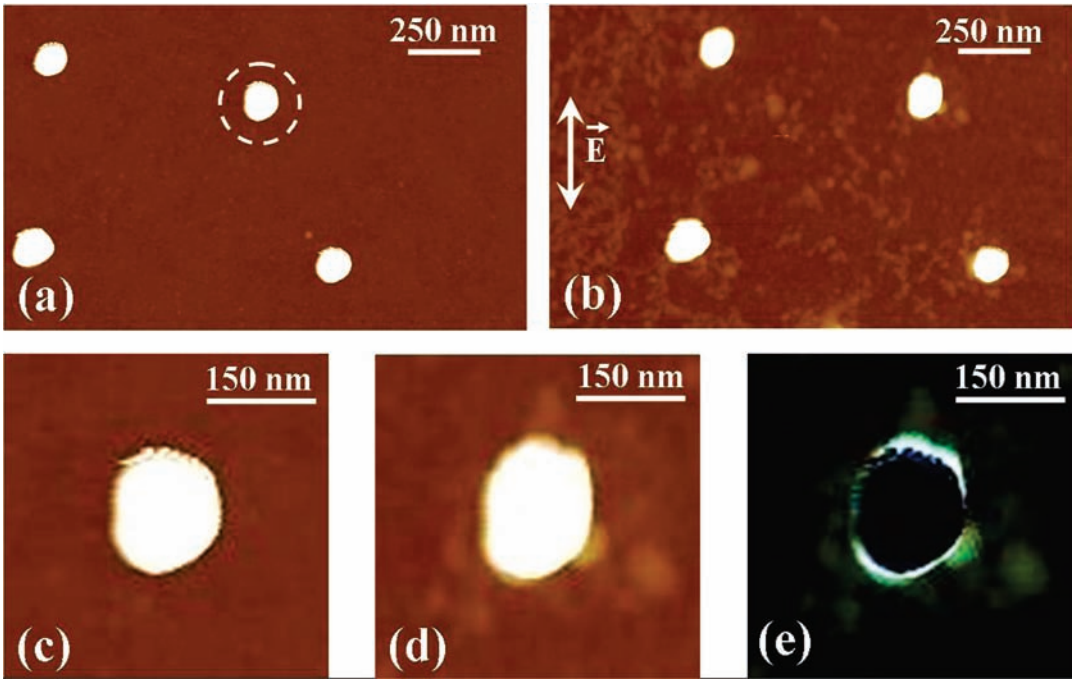

Figure 3. (a,b) AFM images showing the Ag NPs deposited on the functionalized glass substrate, respectively, before and after the procedure. (c,d) Zoom images of the circled particle in panel (a) before the procedure and after the procedure, respectively. The elongation along the vertical direction originates from the formation of polymer lobes. (e) Differential image obtained by subtracting (c) from (d). The incident field polarization direction is indicated by the white vertical arrow shown in panel (b).

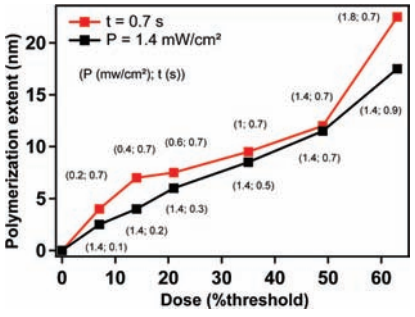

Figure 4. Evolution of the spatial extent of the near-field photopolymerization as a function of relative dose. The black curve shows the polymer width for varying exposure time t (s) at constant power. The red curve illustrates the influence of the incident power P (mW/cm^2) on the polymerization spatial extent for constant irradiation time.

The response of the photochemical system was also evaluated by varying the power and keeping the irradiation time constant to adjust the incident dose between 7% and 63% of the threshold dose. The results at constant time are illustrated by the red curve. Interestingly, the experimental results deviate from those performed at constant power. The deviation indicates that kinetic parameters are governing the lateral extension of the polymerization. The global trend is no longer linear, and polymerization is favored for lower incident power. As expected, the data points overlap for the two curves at $P = 1.4$ mW/cm^2 and $t = 0.7$ s, illustrating both the control and the good reproducibility of our procedure.

At the highest dose (corresponding to 63% of the polymerization threshold), the polymer extent is favored by higher power over longer irradiation time, which is, at a first sight, in contradiction with the results performed at low powers. Because the dose used is close to the threshold, it can be argued that the effect of far-field exposure may no longer be negligible. In particular, an onset of gelification of the medium may perturb diffusion processes at play. For this reason, experiments in the following were systematically carried out at relatively low doses (7% of the threshold dose).

The first conclusion that can be drawn from this study is the clear demonstration that exposure time and irradiation power are not equivalent regarding the spatial extent of the polymerization. To go further into the interpretation of this observation, the conversion of dye and monomer were carried out by UV and FTIR spectroscopy to evaluate the polymerization ratio. Because submicrometer spectroscopic characterization can be conducted only using specific sophisticated configuration (scanning near-field infrared microscopy for instance),[21] we used a simpler approach based on absorption far-field spectroscopy consisting of reproducing the irradiation conditions corresponding to far-field and near-field irradiation. These measurements were conducted on particle-free formulation using two different power densities: the first set of experiment corresponds to 0.1 mW/cm^2, which is an average value for our experiments at the low dose regime. The second intensity used mimics the enhancement effect due to the plasmon excitation at the Ag NP. The enhancement factor was previously determined,[12] and a factor of 20 is commonly admitted. Thus, a second set of spectroscopic characterization was conducted using a power density of 2.00 mW/cm^2. Under such low exposure intensities, local thermal effect and its potential consequences on polymerization kinetics can be neglected, even at the vicinity of the nanoparticles. We note that this macroscopic approach does not take into account factors related to species diffusion. The conversion ratio for the monomer and the bleaching ratio of the dye are plotted in Figure 5 as a function of irradiation time.

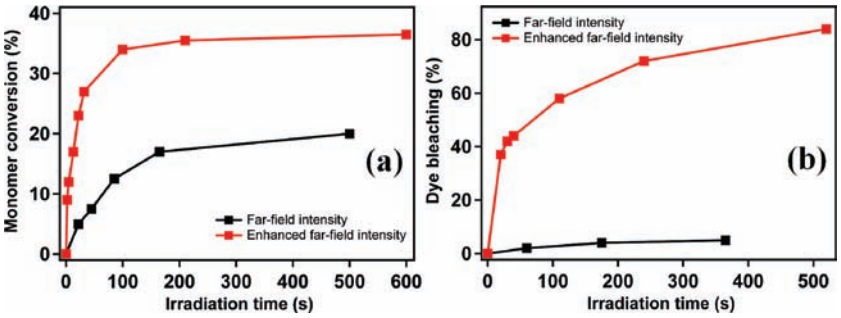

Figure 5. Conversion kinetics of the dye and the monomer in the photopolymerizable solution for two different intensities. The black trace was obtained for an incident power density of $P = 0.10$ mW/cm^2. The red trace was obtained by multiplying the incident power by a factor of 20 ($P = 2.00$ mW/cm^2) to mimic the estimated enhancement factor brought by the surface plasmon excitation. (a) Kinetic of monomer conversion investigated by FTIR and (b) proportion of bleached dye determined by UV−visible spectroscopy evaluated at 532 nm. The threshold time of the formulation was characterized in far-field and was equal to 22 s.

The conversion kinetics of both dye and monomer exhibit significant difference depending on the incident intensity. For intensity corresponding to the far-field exposure represented by the black curves in Figure 5, the conversion of the monomer is very limited (20% after 600 s). Under these conditions, the bleaching ratio remains also at very low level (few %), even for dose much higher than the polymerization threshold. These results demonstrate that at low intensity, molecular modification of the material is negligible. Using these illumination parameters, the threshold of polymerization was observed at 22 s, which corresponds to a monomer conversion of only 5%. One of the characteristics of the monomer that was chosen is indeed to show a very low conversion needed for cross-linking, but sufficient to resist development.

Multiplying the intensity by a factor of 20 to simulate the plasmon enhancement creates a significant modification in the kinetics, as it can be seen in the red curves of Figure 5. A rapid gelification of the photopolymer matrix accounts for a dramatic decrease of the reactive species mobility as soon as the polymerization starts, and thus termination by occlusion process stops the polymerization. However, because the monomer is trifunctional, good mechanical properties are still ensured even for these relatively low conversion percentages. A local enhancement factor of 20 in the vicinity of the nanoparticles is therefore certainly sufficient to initiate a near-field polymerization while preventing a complete polymerization of the formulation. It is worth noticing that the large nonlinearity of the response versus light intensity explains the excellent spatial resolution that is obtained.

The prominent conclusion deduced from this experiment is that the low intensity far-field irradiation does not affect much the global concentration of dye, even with doses leading to a significant bleaching of dye at higher intensity. As discussed in the description of the photopolymerization process, bleaching of eosin by dismutation of eosin radical EH° competes with regeneration. Because the dismutation of eosin is a bimolecular reaction between two protonated eosin radicals, this reaction is favored by a high concentration of these species, which is obtained under high intensity. On the contrary, disproportion reactions with other radical species will be favored when the concentration of protonated eosin radical is at a lower level (i.e., lower intensity). This implies that for low incident powers, bleaching of the eosin is minimal and leads to larger polymerization lobes.

On the basis of these results, the trend observed in Figure 4 can be partially explained: for a given dose, the lateral extent of polymerization is more pronounced for lower intensity. This result is actually in contradiction with previous results reporting on photofabrication on a larger scale[15] where polymerization was significantly favored by an increase of light intensity. This behavior was understood as follows: the inhibition role of oxygen is more pronounced at low intensity (i.e., long irradiation times) because the consumption of oxygen is slow enough to allow for a continual replenishment from the surroundings. The polymerization process starts only when the oxygen concentration in the photopolymer droplet is low enough, which implies that replenishment increases the inhibition time. For higher incident power, the inhibition is less sensitive because diffusion has no time to proceed efficiently. The conclusion of this study is thus exactly opposite to what we observe here at the nanoscale.

A more complete analysis of the involved processes taking place at the nanometer scale needs to be proposed to fully understand the results presented here. Two phenomena are important at this length scale: the diffusion of the dye and the mechanism of eosin regeneration. These two mechanisms strongly depend on the light intensity that governs the polymerization kinetics.

Taking into account that typical dye concentration is 0.5 wt %, and assuming a homogeneous distribution of EY within the photopolymer solution, a volume of $10 \times 10 \times 10$ nm^3 contains only 4 molecules of dye. The same volume contains an average of 200 MDEA molecules and 6000 C═C double bonds. Considering these simple calculations, it appears that the limited reactant is the dye.

Polymerization can only start if the local consumption of oxygen is high enough to efficiently create radicals. Typical oxygen diffusion is about 10^{-12} m^2/s. If one considers that the length over which a species can diffuse is determined by $(Dt)^{1/2}$ where D is the diffusion coefficient and t is the time, the length covered by an oxygen molecule during 1 s is about 1 μm. Local consumption of oxygen is thus very difficult to achieve at the nanoscale. Under these conditions, the extremely limited number of eosin dye as compared to the inhibitor concentration will not lead to polymerization. The local photopolymerization can only be explained by considering the dye diffusion. If the polymerization process is EY diffusion-limited, then an increase of the irradiation time (corresponding to a decrease of the laser intensity by the same factor) is favorable for the polymerization,

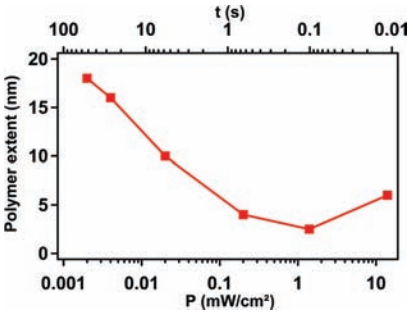

Figure 6. Influence of the incident power (bottom axis) and the exposure time (top axis) on the spatial extent of polymerization. The incident dose is fixed at 7% of the threshold dose.

which will be in accordance with our observed results. Although in microscale photofabrication dye diffusion is usually neglected, this parameter is of critical importance at the nanoscale. Dye diffusion in the monomer matrix is quite slow because of its high molecular weight and polarity. However, by reducing the scale the dye can significantly diffuse in the irradiated volume. Furthermore, the diffusion process can be efficient because bleaching is negligible in the volume corresponding to the optically enhanced region, as it was shown in Figure 5b. In the present case, the diffusion of dye insures a continual replenishment of the volume surrounding the Ag NPs, which partially explains how polymerization can be favored at lower incident powers. Low intensity corresponds to higher irradiation times, which certainly increases the probability of the dye to diffuse in the near-field volume. This discussion is specific to the nanoscale and is linked to the extremely limited number of molecules: at the microscale, the average number of molecules present in the irradiation volume ($1000 \times 1000 \times 1000$ nm^3) is greater by a factor of 10^6, and thus diffusion of the dye from the polymer droplet into the irradiated volume is not predominant. The limiting process at this length scale is the number of photons absorbed by the photopolymer per second, and hence, for a given dose, competitive processes such as inhibition by oxygen are more important.

The second critical parameter involved in the nanoscale enhanced polymerization process relies on the dye regeneration pathways described in Figure 2. As already discussed above, exposure at low intensities favors molecular mechanisms that lead to a regeneration of the eosin in its active form. Consequently, the dye can absorb a new photon and, after reacting with a MDEA molecule, can trigger again a polymerization chain. This hypothesis explains how a very limited number of EY molecules can efficiently initiate the polymerization. Moreover, the very limited number of intermediate species linked to the confinement of the reaction leads to a very low reaction probability between two eosin protonated radicals. Subsequently, dye bleaching in the near-field volume is quite low, and thus one eosin molecule can undergo a large number of cycles before bleaching occurs.

To confirm these assumptions, we investigated the extent of photopolymerization for different intensities at a given dose. The results are plotted in Figure 6. The dose was fixed at 7% of the threshold to avoid far-field polymerization. The curve clearly demonstrates that a decrease of incident power (i.e., an increase of the irradiation time) favors the lateral extent of the polymerization reaction. These data confirm the preliminary conclusion drawn from Figure 4 and emphasize the predominant role of the dye (diffusion and regeneration processes) for controlling the polymerization process. For low intensities, the longer exposures give time for the dye to diffuse from the photopolymer droplet. Because dye consumption by far-field irradiation can be neglected, the droplet constitutes an infinite reservoir of dye. Surprisingly, even for the lowest intensity, the polymerization is not affected by the diffusion of oxygen that acts as an inhibitor.

A different behavior is observed for the last data point (14 mW/cm^2) where a slightly higher polymerization volume was obtained. The effect of oxygen quenching plays an essential role at such high intensity. The corresponding irradiation times are too short to allow for any replenishment of the dye by a diffusion process. Thus, the polymerization is only induced by the excitation of the dyes present in the near-field region at close proximity of the nanoparticle. Notice that for $P = 1.4$ mW/cm^2 and $t = 0.1$ s, the spatial extent of polymerization was extremely limited. Under these conditions and because oxygen diffuses faster than EY, a constant quenching of the reactive species takes place which almost stops the polymerization reaction. When the power is increased from 1.4 to 14 mW/cm^2, the rate of radical production becomes high enough to compete efficiently with oxygen quenching, because O_2 diffusion starts to be time-limited in this last case. Such behavior is in agreement with what is usually observed in photoinduced microfabrication and accounts for the particularity of the last data point in Figure 6.

The processes discussed above are schematically interpreted in Figure 7, showing that polymerization can occur efficiently only when the level of dye is greater than that of the inhibitor. The figure illustrates the spatial distribution of the dye and O_2 concentration in stationary state deduced from the polymerization profiles for different intensities. Figure 7a sketches the spatial distribution of the electromagnetic field around the nanoparticle and the level of far-field excitation. Figure 7b shows the effect of a low intensity irradiation corresponding to a long exposure time. In this case, the dye concentration in the near-field volume is slightly lower than the EY bulk concentration because of diffusion process, and the conditions are favorable for eosin regeneration. Under such circumstances and as long as gelification is not occurring, the concentration of the dye remains at a relatively high level. Reactive species can be created at a rate high enough to counterbalance the oxygen inhibition, despite the continual supply of O_2 by diffusion. This actually induces a low O_2 concentration close to the Ag NPs, which then trigger polymerization. In the case of Figure 7c (average intensity), the polymerization in the near-field excitation volume is reduced because the dye does not have the time to diffuse in the volume. However, the exposure time is still long enough to keep the oxygen concentration at a value sufficient to quench the polymerization. An increase of the intensity (Figure 7d) reduces the local concentration of O_2 to an extremely low value, ensuring polymerization to occur.

To state the role of EY diffusion, the same experiments were conducted using a formulation with a dye concentration divided by a factor of 5 (0.1 wt %). Figure 8 shows a comparison between the measured lateral extents of the polymer lobes for the two dye concentrations. Exposures were conducted at 7% of the threshold doses determined independently for both formulations.

The decrease of the eosin concentration in the formulation leads to a decrease of the polymerization process for all irradiation times. These results illustrate the clear effect of the dye concentration on the polymerization extent. Accordingly, the

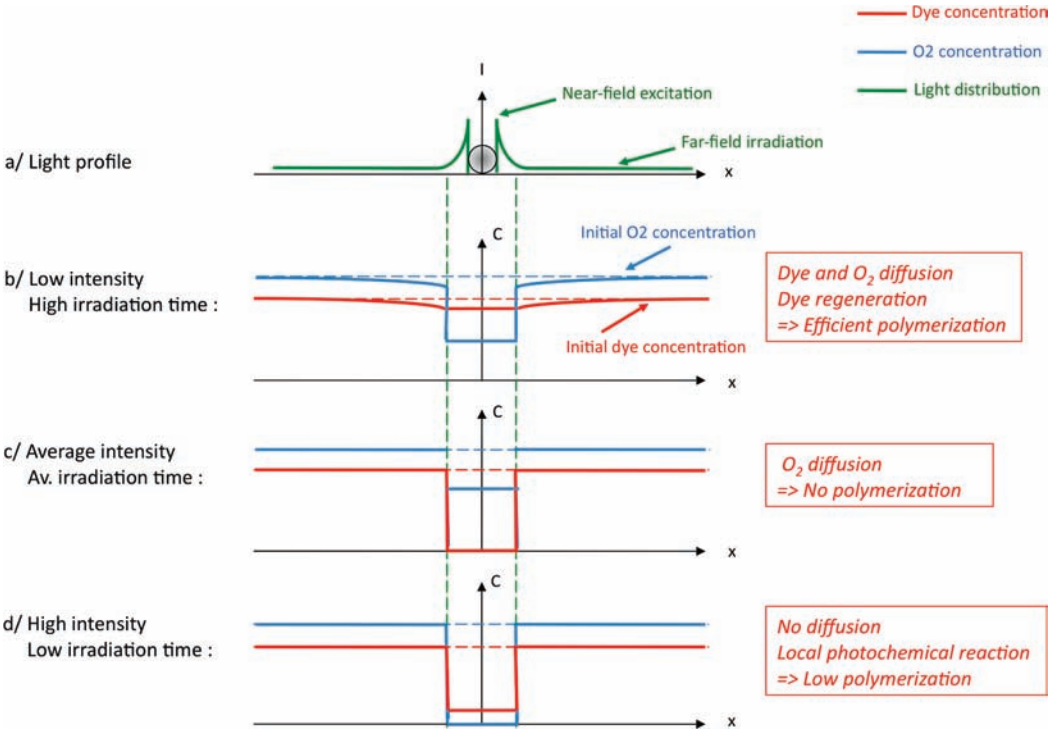

Figure 7. Schematic repartition of the dye and O_2 concentration around the Ag NPs for different polymerization regimes. Panel (a) corresponds to the spatial distribution of the electromagnetic field, indicating the level of both the far-field and the enhanced near-field intensities. Panels (b−d) correspond respectively to low, average, and high intensity (respectively, high, average, and low irradiation time), as defined by the three regimes observed in Figure 6. The comparison of the local concentration between dye and inhibitor (oxygen) indicates the degree of polymerization.

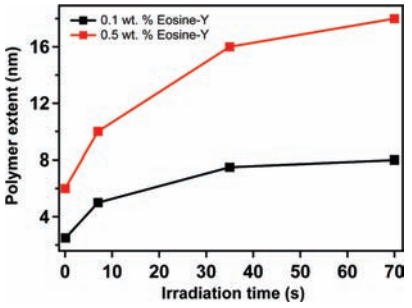

Figure 8. Role of EY concentration on the spatial extent of the polymerization. Dye concentrations at 0.5 and 0.1 wt % were used. The MDEA concentration is fixed at 4 wt %, and the incident dose is kept constant for both experiments at a value equal to 7% of the polymerization threshold (evaluated separately for each formulation).

local concentration of EY is a critical factor limiting the polymerization process. It was not possible to test higher dye concentrations because 0.5 wt % is close to the eosin solubility in the formulation. The minimum measured polymer width is 2 nm for the formulation containing 0.1 wt % of EY, and a plateau is observed at 8 nm after 30 s. Using this saturation effect, the dimensions of the polymer lobes are almost independent of the irradiation conditions. This clearly indicates that lower dye concentration is favorable if high resolution is needed.

CONCLUSIONS

This Article proposes a new approach for fabricating hybrid nanostructures by local surface-plasmon-based photopolymerization. We unambiguously demonstrate the creation of polymer structures down to a size of a few nanometers by relying on the optical properties of metal nanoparticles excited close to their plasmon resonance.

Our investigations show that polymerization at the nanoscale is governed by photochemical parameters. In particular, we demonstrated that chemical kinetics are specific to this length scale and cannot be simply extrapolated from microscale considerations. The extreme confinement of the excitation volume offers a unique perspective for investigating photochemistry occurring at this length scale. We showed that diffusion processes are playing a major role in the polymerization because migration of the molecules at the nanoscale requires times much smaller than the irradiation time. Consequently, diffusion and reaction processes are competing, and the results are strongly affected by the intensity used for photofabrication. Furthermore, the extremely limited number of chemical species contained in the irradiated volume implies that all of the photochemical pathways are of importance in the process. This is particularly the case for the regeneration routes of eosin because they favor polymerization.

Because the plasmon resonance of metal nanoparticles can be precisely tailored by changing the morphology, our approach can be applied to different photosensitive formulations. This will help to discriminate between the relative contributions of diffusion and regeneration in the photopolymerization process occurring at the nanoscale. Furthermore, the field distributions around nanoparticles can also be designed to create more complex nanostructures. The resolution obtained with this approach proposes a valuable alternative route for fabricating nanostructures.

AUTHOR INFORMATION

Corresponding Author
olivier.soppera@uha.fr; renaud.bachelot@utt.fr

ACKNOWLEDGMENT

We thank the Agence Nationale de la Recherche (ANR), under Grant Photohybrid (BLANC 07-2-188654), for financial support. This work was also partially supported by the Partner University Funds program (PUF 2010).

REFERENCES

(1) Nie, Z.; Kumacheva, E. *Nat. Mater.* **2008**, *7*, 277–290.
(2) Scott, T. F.; Kowalski, B. A.; Sullivan, A. C.; Bowman, C. N.; McLeod, R. R. *Science* **2009**, *324*, 913–917.
(3) Li, L.; Gattass, R. R.; Gershgoren, E.; Hwang, H.; Fourkas, J. T. *Science* **2009**, *324*, 910–913.
(4) Andrew, T. L.; Tsai, H. Y.; Menon, R. *Science* **2009**, *324*, 917–921.
(5) Hell, S. W. *Nat. Methods* **2009**, *6*, 24–32.
(6) Maier, S. *Plasmonics: Fundamentals and Applications*; Springer: New York, 2007.
(7) Viste, P.; Plain, J.; Jaffiol, R.; Vial, A.; Adam, P. M.; Royer, P. *ACS Nano* **2010**, *4*, 759–764.
(8) Noginov, M. A.; Zhu, G.; Belgrave, A. M.; Bakker, R.; Shalaev, V. M.; Narimanov, E. E.; Stout, S.; Herz, E.; Suteewong, T.; Wiesner, U. *Nature* **2009**, *460*, 1110–1112.
(9) Berthelot, J.; Bouhelier, A.; Huang, C.; Margueritat, C.; Colas-des Francs, G.; Finot, E.; Weeber, J.; Dereux, A.; Kostcheev, S.; Ahrach, H. I.; Baudrion, A. L.; Plain, J.; Bachelot, R.; Royer, P.; Wiederrecht, G. *Nano Lett.* **2009**, *9*, 3914–3921.
(10) Barbillon, G.; Bijeon, J. L.; Plain, J.; Lamy De La Chapelle, M.; Adam, P. M.; Royer, P. *Gold Bull.* **2007**, *40*, 240–244.
(11) Ibn El Ahrach, H.; Bachelot, R.; Vial, A.; Lerondel, G.; Plain, J.; Royer, P.; Soppera, O. *Phys. Rev. Lett.* **2007**, *98*, 107402.
(12) Deeb, C.; Bachelot, R.; Plain, J.; Baudrion, A. L.; Jradi, S.; Bouhelier, A.; Soppera, O.; Jain, P. K.; Huang, L.; Ecoffet, C.; Balan, L.; Royer, P. *ACS Nano* **2010**, *4*, 4579–4586.
(13) Ueno, K.; Juodkazis, S.; Shibuya, T.; Yokota, Y.; Mizeikis, V.; Sasaki, K.; Misawa, H. *J. Am. Chem. Soc.* **2008**, *130*, 6928–6929.
(14) Mandal, T. K.; Fleming, M. S.; Walt, D. R. *Nano Lett.* **2002**, *2*, 3–7.
(15) Soppera, O.; Jradi, S.; Lougnot, D. J. *J. Polym. Sci., Part A: Polym. Chem.* **2008**, *46*, 3783–3794.
(16) Jradi, S.; Soppera, O.; Lougnot, D. J. *J. Microsc.* **2008**, *229*, 151–161.
(17) Carre, C.; Lougnot, D. J.; Renotte, Y.; Leclere, P.; Lion, Y. *J. Opt.* **1992**, *23*, 73.
(18) Decker, C.; Jenkins, A. D. *Macromolecules* **1985**, *18*, 1241–1244.
(19) Fouassier, J. P.; Chesneau, E. *Makromol. Chem.* **1991**, *192*, 245–260.
(20) Avens, H. J.; Bowman, C. N. *J. Polym. Sci., Part A: Polym. Chem.* **2009**, *47*, 6083–6094.
(21) Wollny, G.; Bründermann, E.; Arsov, Z.; Quaroni, L.; Havenith, M. *Opt. Express* **2008**, *16*, 7453–7459.